Electronic Supplementary Information

Topography-guided buckling of swollen polymer bilayer films into three-dimensional structures

Joonwoo Jeong, Yigil Cho, Su Yeon Lee, Xingting Gong, Randall D. Kamien, Shu Yang, and A. G. Yodh

Reproducibility after de-swelling and re-swelling

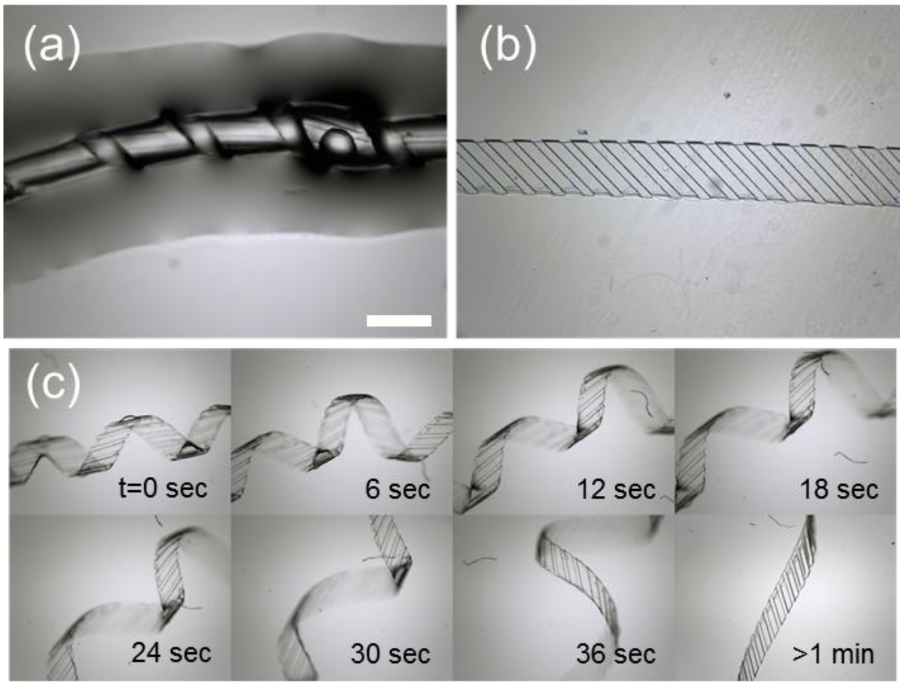

Fig. S1. De-swelling of a bilayer strip soaked in hexadecane. (a) A swollen strip from a hexadecane bath is place on a substrate. Scale bar: 300 μm. (b) The strip in (a) after washing with ethanol. (c) De-swelling process of a hexadecane-swollen strip in an ethanol bath. The helical ribbons unwinds and straightens as time goes by.

In Fig. S1(a), we show a swollen strip taken out of a hexadecane bath and placed on a glass substrate. Since the vapor pressure of hexadecane is low, the strip maintains its helical ribbon shape unless the hexadecane is washed out. Fig. S1(c) shows snapshots of the same strip during the process of de-swelling in the ethanol bath. Ethanol dissolves hexadecane, swells the PDMS negligibly, and dries quickly. The helical ribbon unwinds slowly and becomes almost a flat strip. However, the ribbon is not completely flat due to either swelling by the ethanol or to a residual stress in the parylene film. The ethanol-washed strip can be dried on a substrate in a flat configuration and thus be made ready for re-swelling, as shown in Fig. S1(b).

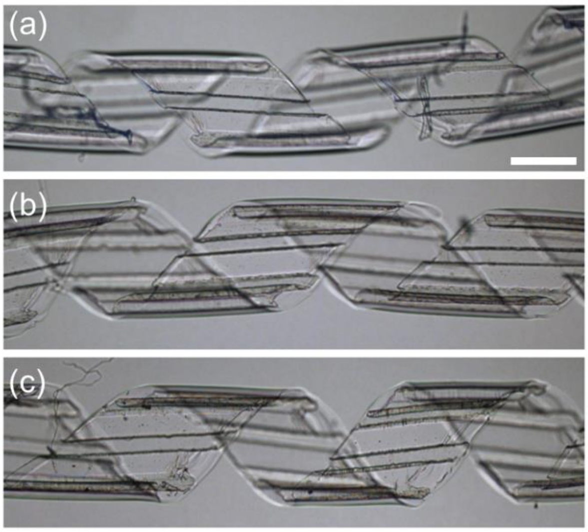

Fig. S2. Repeated swelling of a bilayer strip. (a)-(c) Swollen configurations of a bilayer strip after the first, second, and third swelling, respectively. Scale bar: 300 μm. Note, the images were taken from the same strip after each swelling, but were not taken from the same part of the strip. Additionally, all the helical ribbons are right-handed; the ribbon in Fig. S2(a) looks different from the others, because the image is obtained from a different focal plane.

To demonstrate reproducibility, we repeated the swelling of a single strip three times, as shown in Fig. S2. Each swelling was followed by de-swelling. We confirmed the ridge and valley align along the helical axis even after the repeated swelling, as our model predicts. We found that the diameter of the helical tubule, however, increases approximately by 10% after the first swelling. Because a larger diameter means less stress, we presume the first contact with the swelling solvent, *i.e.*, hexadecane, permanently changes properties of a bilayer strip, *i.e.*, its swelling ratio by dissolving out un-crosslinked components. Alternatively, a remnant of the de-swelling solvent, *i.e.*, ethanol, in the PDMS may affect the re-swelling.

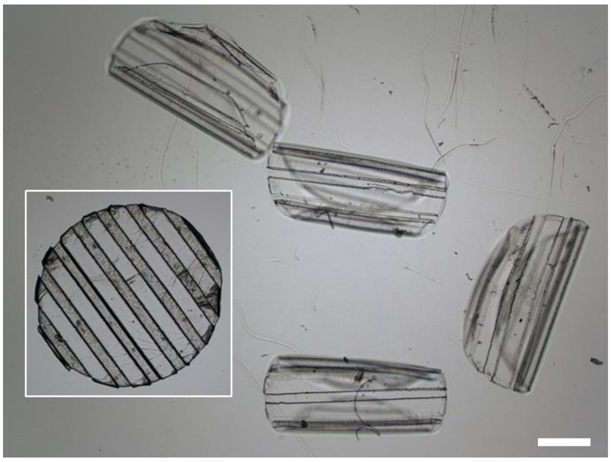

Fig. S3. Swollen disks in a “taco” shape. Scale bar: 300 μm. (Inset) A punch-cut disk in a flat configuration before swelling.

Reproducibility within a batch is shown with Fig. S3. Because it is difficult to produce identical strips by manual cutting, we used a biopsy punch of 1 mm diameter to make disks for a single sheet; their swollen configurations, “tacos”, are shown in Fig. S3. Note that the “tacos” have different viewing angle but almost identical shapes.

Control experiments to show the role of topography

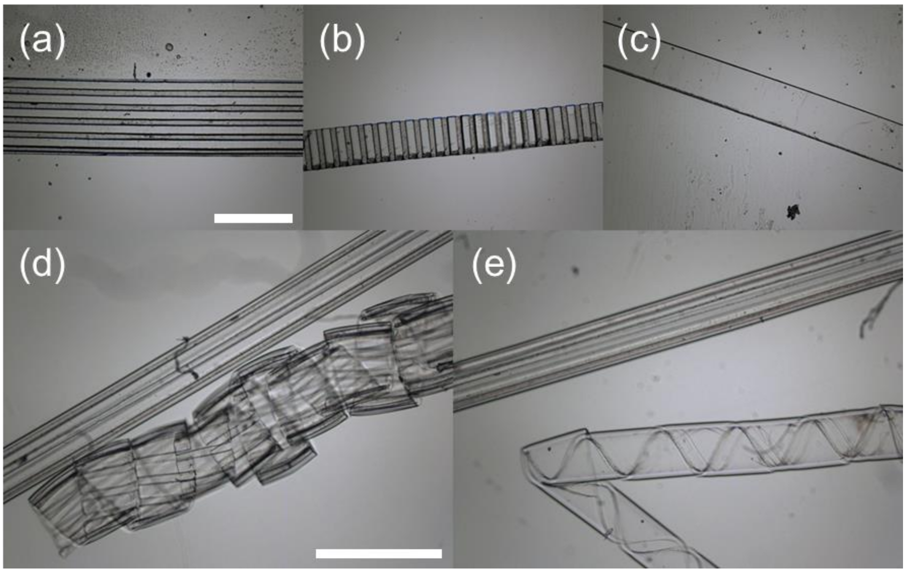

Fig. S4. Different shapes of swollen strips manifesting the role of topography. (a)-(c) Ethanol-washed strips in flat configuration on a substrate. Scale bars: 1 mm. Ridges/Valleys are parallel to the strip in (a) and perpendicular to the strip in (b). The strip in (c) has no topographic structure. (d) The straight half-pipe results from swelling of (a), and the self-interacting "roll" results from swelling of (b). (e) The bilayer strip without topography, (c), also buckles into a helical tubule (Bottom). But the buckling is not guided, so that the shapes it develops into are irregular and uncontrolled.

Fig. S4 provides the results of control experiments to demonstrate the role of topography. Namely, swelling of a flat bilayer strip without topography (Fig. S4(c)) is compared to two other extreme cases with topography. As shown in Fig. 4(a), (b), and (d), the bilayer strips with ridges parallel or perpendicular to the strips result in a straight half-pipe and a self-interacting "roll", respectively, where the ridges/valley are parallel to the direction of zero curvature as expected. By contrast, as shown in Fig. 4(e), the strip without guiding topography buckles into a self-interacting and irregular helical tubule.

Solutions for the geometric model of helical ribbons with parylene on the flat side of topographically patterned PDMS films.

In Fig. S5(a), we show example contour plots of Equation 3 and Equation 4 of the main text. In other words, the r and β on the green curve satisfy Equation 3, which characterizes the constraint that the length of the PDMS strip, $L_{out,}$ expands to match λL. The points on the red curve satisfy a constraint that the length of ridges located outside of the helical ribbon, $L_{R,out}$, will swell to match λL_R. Thus, the two points of intersection between the green and red curves are solutions that meet both constraints. Note, they represent purely geometric solutions. In practice, we expect/assume that the solution with a larger radius (Fig. S5(c)), and thus a smaller bending energy, leads to a helical ribbon close to the observation (Fig. S5(d)).

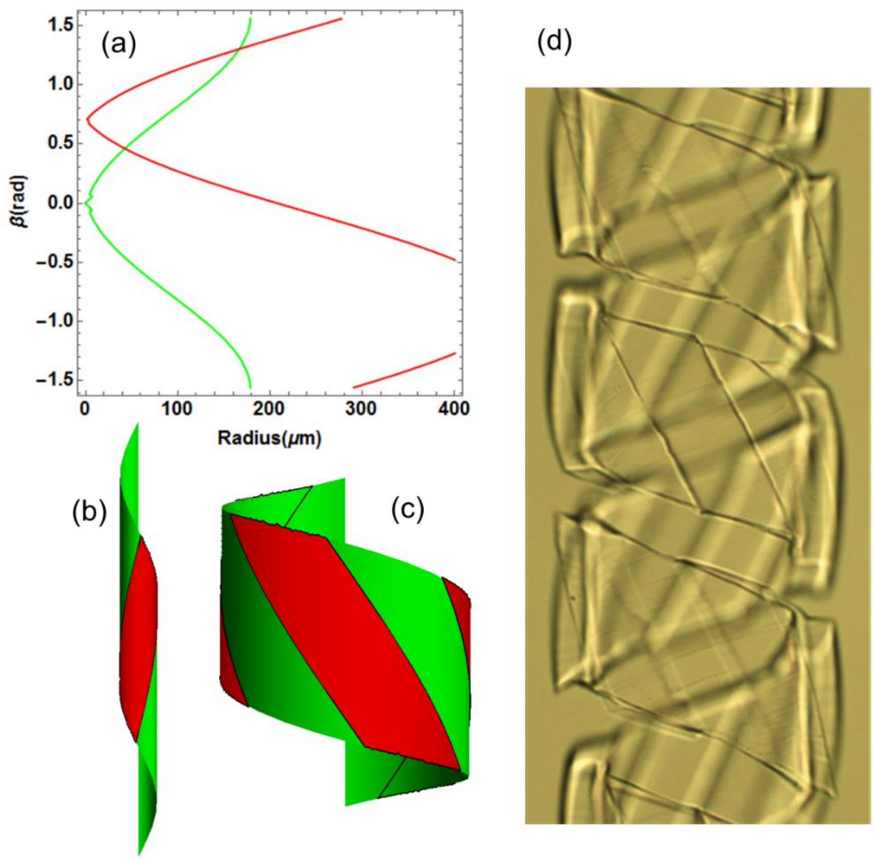

Fig. S5. Comparison of geometric model solutions with an experimental result. (a) Example contour plots of Equation 3 (Green) and Equation 4 (Red) in the main text and. Two cross points correspond to two sets of solutions, r and β, which can simultaneously satisfy Eq. (3) and (4). Here the effective swelling ratio, λ= 1.14, and the ridge angle, α= 50 ^{o}. T'_R and T'_V are 40 μm and 25 μm, respectively. (b) and (c) correspond to two sets of solutions in (a) with the smaller radius and the larger radius, respectively. The width of the ridge region (red) is 100 μm. (d) Optical microscopy image of the corresponding bilayer strips in its swollen state placed in a solvent.

Derivation of equations calculating lengths on the helical ribbon

Because it is intrinsically flat, the distance between two points on a cylindrical surface can be calculated by unrolling the curved surface onto the corresponding planar surface. On the planar surface, the distance is simply determined from the Pythagorean sum of the lengths of two orthogonal components: the arc length and the length along the cylindrical axis, as shown in Fig. S6. Notice, also, that while the length measured along the cylindrical axis is independent of the radius of the cylinder, the arc length depends on the radius. Consider a cylindrical shell with inner and outer radii, for example; in this case, the length of a line on the outer surface is different from the length of its projection onto the inner surface, because they have different arc-length components.

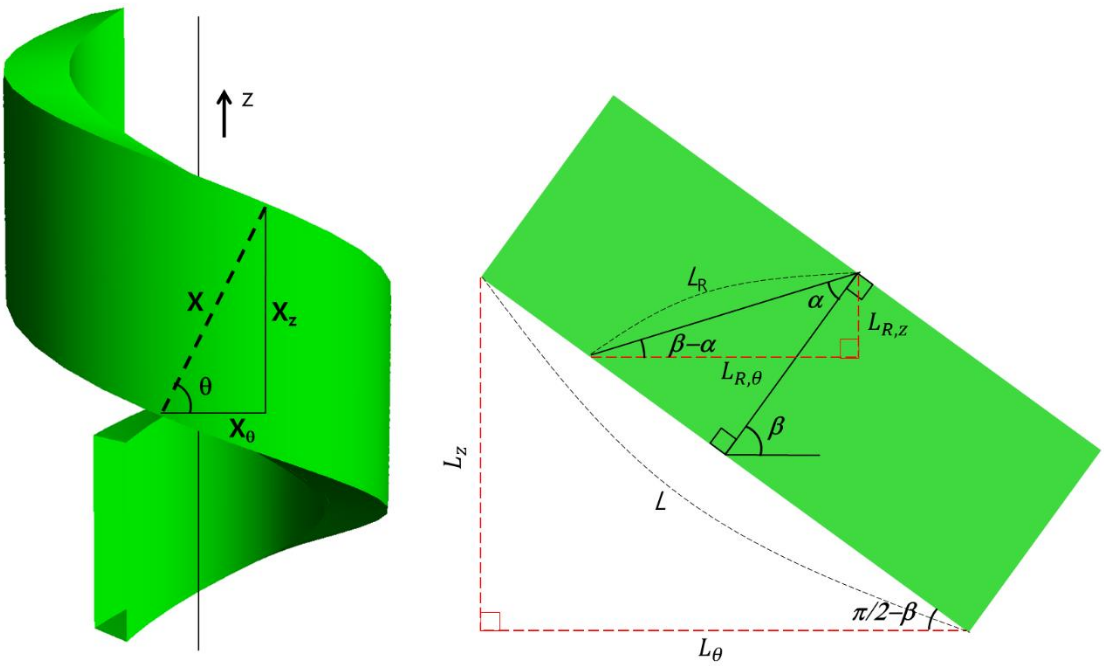

Fig. S6. A 3D perspective view (Left) and a planar figure (Right) of a helical ribbon. The side (Left) and top (Right) view. L_z is parallel to the cylindrical axis.

Lengths on the helical ribbon with the same zero Gaussian curvature are readily calculated. Fig. S6 shows the planar figure of the helical ribbon. For the case of the bilayer strip with parylene-C deposited on the patterned side, *i.e.*, Fig. 3(b) in the main text, the flat side is located outside of the ribbon. The radius of curvature of this flat side is r, and the radius of curvature of the patterned surface, located on the cylindrical shell's inner side, is r-T'_v. When L_z is the length component along the cylindrical axis, then both inner and outer sides also have a length component L_z. However, L_θ of the outer side is longer than the corresponding length on the inner side, *i.e.*, by the factor $r/(r-T'_v)$. The length along the flat side, L_{flat}, is the Pythagorean sum of $L_{flat,z}$ and $L_{flat,\theta}$ and it can be expressed in terms of L_{valley}, $L_{valley,z}$ and $L_{valley,\theta}$ that are lengths on the cylindrical plane where the valley is located.

$$L_{flat} = \sqrt{L_{flat,z}^2 + L_{flat,\theta}^2} = \sqrt{L_{valley,z}^2 + \left(\frac{r}{r-T_v'}L_{valley,\theta}\right)^2} = L_{valley}\sqrt{\sin^2(\frac{\pi}{2}-\beta) + \left(\frac{r}{r-T_v'}\cos(\frac{\pi}{2}-\beta)\right)^2}.$$

L_R can be written using the Pythagorean sum in the similar way.

$$L_{R,ridge} = \sqrt{L_{R,ridge,z}^2 + L_{R,ridge,\theta}^2} = \sqrt{L_{R,valley,z}^2 + \left(\frac{r-T_R'}{r-T_V'}L_{R,valley,\theta}\right)^2} = L_{R,valley}\sqrt{\sin^2(\beta-\alpha) + \left(\frac{r-T_R'}{r-T_V'}\cos(\beta-\alpha)\right)^2}.$$